A folding-dependent mechanism of antimicrobial peptide resistance to degradation unveiled by solution structure of distinctin

Domenico Raimondo*†, Giuseppina Andreotti*†, Nathalie Saint†‡, Pietro Amodeo*†, Giovanni Renzone§, Marina Sanseverino¶, Ivana Zocchi¶, Gerard Molle‡, Andrea Motta*, and Andrea Scaloni§∥

*Institute of Biomolecular Chemistry, National Research Council, Comprensorio Olivetti, Edificio 70, I-80078 Pozzuoli (Naples), Italy; ‡Centre de Biochimie Structurale, Unité Mixte de Recherche 5048 Centre National de la Recherche Scientifique, U554 Institut National de la Santé et de la Recherche Médicale, F-34090 Montpellier, France; §Proteomics and Mass Spectrometry Laboratory, Istituto per il Sistema Produzione Animale in Ambiente Mediterraneo (ISPAAM), National Research Council, I-80147 Naples, Italy; and ¶INBIOS S.r.l., Via Olivetti 1, I-80078 Pozzuoli (Naples), Italy

Many bioactive peptides, presenting an unstructured conformation in aqueous solution, are made resistant to degradation by posttranslational modifications. Here, we describe how molecular oligomerization in aqueous solution can generate a still unknown transport form for amphipathic peptides, which is more compact and resistant to proteases than forms related to any possible monomer. This phenomenon emerged from 3D structure, function, and degradation properties of distinctin, a heterodimeric antimicrobial compound consisting of two peptide chains linked by a disulfide bond. After homodimerization in water, this peptide exhibited a fold consisting of a symmetrical full-parallel four-helix bundle, with a well secluded hydrophobic core and exposed basic residues. This fold significantly stabilizes distinctin against proteases compared with other linear amphipathic peptides, without affecting its antimicrobial, hemolytic, and ion-channel formation properties after membrane interaction. This full-parallel helical orientation represents a perfect compromise between formation of a stable structure in water and requirement of a drastic structural rearrangement in membranes to elicit antimicrobial potential. Thus, distinctin can be claimed as a prototype of a previously unrecognized class of antimicrobial derivatives. These results suggest a critical revision of the role of peptide oligomerization whenever solubility or resistance to proteases is known to affect biological properties.

NMR structure | oligomerization | pore-forming peptide | disulfide

Antimicrobial cationic peptides are essential effector molecules of the innate immune system in multicellular organisms, which provide protection against microbial pathogens (1, 2). Larger precursors are synthesized by ribosomes, proteolytically cleaved into compounds comprising 10–60 aa, and eventually affected by C-terminal amidation, amino acid isomerization, or cysteine pairing. Hundreds of antimicrobial peptides have been discovered so far, and they have been classified according to their sequence similarity, secondary structure content, and number of disulfide bonds (1, 2). In general, most of these molecules assume a conformation in which clusters of hydrophobic and cationic amino acids are spatially organized into discrete sectors of the molecule, determining the so-called amphipathic design. This peculiar feature is responsible for their interaction with microbial membrane, a cellular compartment where their function seems to be accomplished by permeation processes.

Amphibian skin is one of the richest sources of antimicrobial peptides. Frogs and toads are known to secrete from dorsal granular glands two main classes of these compounds (1–4). The first group includes linear peptides with no cysteines that form an amphipathic α-helical structure in hydrophobic environment (1–5). The second class comprises peptides presenting a C-terminal S–S bridge, which generates a 7- to 9-aa cyclic moiety

(1, 4). Recently, different antimicrobial molecules with intriguing structural features have been discovered (6). Among these, distinctin (D1), a bioactive peptide purified from *Phyllomedusa distincta*, has been demonstrated to present an uncommon heterodimeric structure consisting of two different polypeptide chains linked by a disulfide bond (7). Antimicrobial assays have shown that D1 is active against pathogenic bacteria. Its lytic activity on large unilamellar vesicles suggested a specific action on cellular membranes. Conformational investigations indicated an increase in α-helical content when D1 was transferred into a membrane-like environment.

Recently, other hetero- and homodimeric peptides with bactericidal properties have been isolated in hemocytes of *Halocynthia aurantium* (8, 9) and mouse intestinal tissues (10), namely dicynthaurin, halocidin, and cryptidin-related sequence peptides. Spectroscopic analysis has demonstrated that dicynthaurin and halocidin have a propensity to assume an α-helical conformation; the others are highly homologous to peptides with a relatively rigid antiparallel β-sheet structure. Animal peptides with a dimeric structure stabilized by a disulfide bond are rare, and D1, together with the above-mentioned molecules, may be an example of a previously unrecognized class of antimicrobial compounds. To definitively characterize the conformational properties and elucidate the mechanism of action, we have determined the 3D structure of D1 in aqueous solution and studied its ability to form pores in biological membranes.

Materials and Methods

Peptide Synthesis and Biological Assays. Peptides were synthesized, characterized, and tested for their biological and biophysical activity as reported in *Supporting Materials and Methods*, which is published as supporting information on the PNAS web site.

NMR Spectroscopy. NMR samples were prepared by dissolving D1 in 90% ^1H_2O/10% ^2H_2O (vol/vol) or 100% ^2H_2O. Experiments were performed with 0.05 and 3.80 mM peptide concentrations, at pH 5.8 and 6.8 and at 300 and 310 K, as reported in *Supporting Materials and Methods*.

Peptide Degradation. Comparative proteolysis experiments on melittin, magainin II, D1 chain A, D1 chain B, and intact D1

BIOPHYSICS

Table 1. Minimal inhibitory concentration of natural and synthetic D1 compared with other antimicrobial compounds

| Antibiotic | Minimal inhibitory concentration, μM | | | |
	Escherichia coli	Staphylococcus aureus	Pseudomonas aeruginosa	Enterococcus faecalis
Natural D1	14.5	29.0	29.0	14.5
Synthetic D1	14.5	29.0	29.0	14.5
Ampicillin	50	<0.7	>100	ND
Melittin	0.35	0.17	2.8	ND
Magainin II	0.8	51.8	25.9	>51.8
Ranalexin	15.2	3.8	60.8	60.8
Cecropin A	0.5	32.0	8	>32.0

ND, not determined.

molecule were performed in parallel, incubating each peptide (300 pmol) in 50 mM ammonium acetate, pH 6.5, at 37°C, with equal amounts of subtilisin, chymotrypsin, or trypsin. Added enzyme amounts ranged from 15 to 0.09 ng. Aliquots (30 pmol) were withdrawn on a time-course basis and directly analyzed by MALDI-TOF MS, as reported in ref. 11.

Results

Synthesis and Antimicrobial and Hemolytic Activity. D1 was synthesized by a solid-phase strategy, as described in *Supporting Materials and Methods*. Disulfide bonds were formed by air oxidation of unprotected thiols in a basic aqueous solution. This procedure gave a yield of 80.3%, demonstrating that heterodimeric oxidation was preferred to homodimeric one. HPLC and MS analysis confirmed that synthetic peptide was identical to natural one (Fig. 4, which is published as supporting information on the PNAS web site). Furthermore, CD analysis of natural and synthetic D1 in water and trifluoroethanol afforded spectra almost undistinguishable and fully superimposable to those already reported (7), suggesting that the two peptides adopted an identical conformation in the same solvents.

Natural and synthetic D1 were also tested for their activity against pathogenic Gram-positive and Gram-negative bacteria. In this case also, identical results were obtained. These data were compared with those determined in parallel for other peptides known for their marked antimicrobial activity (Table 1). These experiments demonstrated that D1 is capable of inhibiting bacterial growth with an efficacy similar to other antibiotics.

We also evaluated the ability of D1 to disrupt human erythrocyte membranes. In this case, D1 was tested in a comparative analysis with melittin; as expected, activity profiles generated for synthetic and natural D1 were totally superimposable (not shown). Moreover, D1 was significantly less effective than melittin in permeabilizing erythrocytes (Fig. 1*A*). In fact, even at 200 μM, D1 could not significantly disrupt erythrocyte membranes (<5%). These results were very similar to those reported for dicynthaurin and halocidin (8, 9), suggesting a common specificity of these peptides toward bacterial membranes.

Ion-Channel Formation. Although the exact mechanism by which some antibiotics (Table 1) kill bacteria is not fully understood, it has been shown that peptide–lipid interactions leading to membrane permeation play a role in their activity. Macroscopic and single-channel experiments have been used to screen the functional properties of potential pore-former compounds (5, 12). Thus, synthetic D1 was incorporated into asolectin or phosphatidylcholine/phosphatidylethanolamine planar bilayers, which were submitted to repetitive voltage ramps. It was necessary to impose high voltages (>200 mV) to incorporate peptide into bilayers. After 15 min, an I–V curve was obtained (Fig. 1*B*). The exponential development of membrane current observed above a voltage threshold
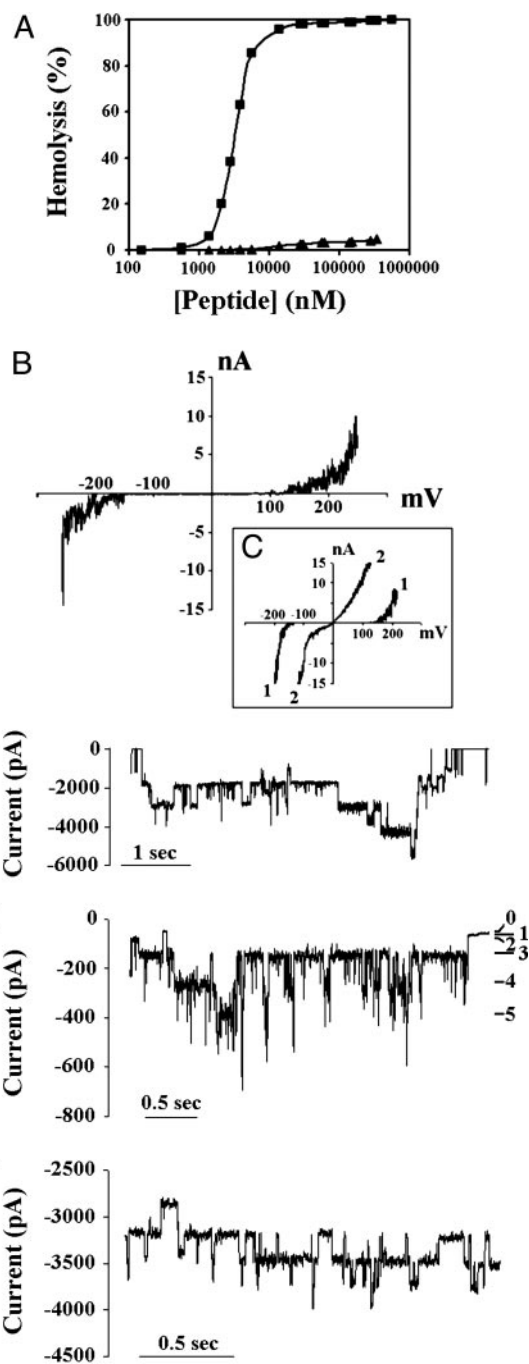
Fig. 1. D1 activity on natural and synthetic membranes. (*A*) Hemolytic activity of D1 (▲) and melittin (■) on human erythrocytes. Each value corresponds to the mean of three experiments done in duplicate. (*B–F*) Macroscopic (*B* and *C*) and single-channel (*D–F*) experiments with D1. (*B*) Current–voltage (*I–V*) curve between −250 and +250 mV at a ramp sweep of 10 mV/sec, 15 min after incorporation of D1 (30 nM), in asolectin (soybean phospholipid) membranes. (*C*) *I–V* curve at the same ramp sweep after 20 min (curve 1) and 45 min (curve 2). Measurements were performed in 10 mM Hepes/1 M KCl, pH 7.4, at 25°C. (*D–F*) Single-channel traces induced by D1 (10 nM) in a phosphatidylcholine/phosphatidylethanolamine bilayer formed at the tip of patch clamp pipette in 1 M KCl, at 25°C. Digitization rate, 5 kHz; filter, 1 kHz. (*D*) At 250 mV after 10 min. (*E*) At 84 mV after 1 h. The strokes in the right part indicate the different sublevels. (*F*) At 160 mV after 2 h.

was characteristic of a voltage-dependent behavior. However, the voltage threshold shifted quickly to lower voltage values and I–V curves became practically ohmic (Fig. 1*C*).

Table 2. Single-channel conductance levels of D1 in phosphatidylcholine/phosphatidylethanolamine membranes

	Conductance, pS							
V, mV	1	2	3	4	5	6	7	8
50	50	280	580	1,260	2,700			
80	70	220	540	1,450	2,800	4,200		
160	—	—	560	1,540	2,750	4,435	6,100	8,010
250	—	—	—	1,400	2,580	4,300	5,900	7,800
140	*—*	*170*	*400*	*1,300*	*2,500*	*4,000*	*5,600*	*7,200*

The values measured for alamethicin are in italic.

Single-channel experiments (13, 14) also required high voltages (250 mV) to induce ion channel formation, just after peptide incorporation (Fig. 1*D*). As soon as D1 aggregates were incorporated into bilayers, it was possible to obtain well defined single channels at lower voltages. The trace obtained at 84 mV after 1 h (Fig. 1*E*) showed typical current profiles indicating a multistate behavior. Experiments performed on a large scale of voltages showed a geometrical progression of increments between the average conductance (Table 2). A comparison of conductance sublevels with those obtained for alamethicin demonstrated a similar behavior of these peptides. If the voltage was under 100 mV, the lower levels of current could be observed. When the voltage increased, a shift of levels occurred to the larger conducting aggregates, as shown by the trace recorded after 2 h (Fig. 1*F*), with the fluctuating levels between 2 and 4

nA. The strong interaction between negatively charged phospholipid head-groups and cationic residues is an important step in membrane permeation of antimicrobial peptides from amphibian skin (1–4). To test the eventual role of negatively charged lipids on D1 properties, other experiments were performed into phosphatidylcholine/phosphatidylethanolamine/phosphatidylserine bilayers at various voltages. These experiments showed that D1 displayed the same behavior with this mixture of lipids (not shown).

Secondary Structure of D1. The detailed structure of D1 in aqueous solution was determined by NMR spectroscopy. Total correlation spectroscopy (TOCSY) and NOESY spectra were recorded and processed (Table 4, which is published as supporting information on the PNAS web site). The secondary structure of D1 was determined by qualitative analysis of the sequential (αCH_i–NH_{i+1} and NH_i–NH_{i+1}) and medium-range (αCH_i–NH_{i+n}, $1 < n < 4$, and αCH_i–βCH_{i+3}) nuclear Overhauser enhancements (NOEs), and from $^3J_{HN\alpha}$ coupling constants (Fig. 5*A*, which is published as supporting information on the PNAS web site). The presence of strong NH_i–NH_{i+1} NOEs and weak αCH_i–NH_{i+1} cross-peaks in the G^{8A}–C^{19A} region of chain A and the G^{5B}–C^{23B} region of chain B suggested an α-helical conformation. This finding was supported by several unambiguous αCH_i–NH_{i+3}, βCH_i–NH_{i+1}, αCH_i–βCH_{i+3} and αCH_i–NH_{i+4} cross-peaks. A set of 88 H-bond restraints (9 O_i–N_{i+4} and 9 O_i–HN_{i+4} distances for each A chain, 13 O_i–N_{i+4} and 13 O_i–HN_{i+4} distances for each B chain), to be used in the subsequent structural determination, was derived from these results.

Table 3. Structural statistics for the bundle of 24 selected D1 structures

Experimental restraints				
I-residue NOEs	16			
i-residue sNOEs ($\|i - j\| = 1$)	312			
i-residue mrNOEs ($1 < i - j \leq 5$)	170 (I-chain A_i–A_i or B_i–B_i)			
i-residue lrNOEs ($\|i - j\| > 5$)	50 (16 i-chain I-mol A_i–B_i, 34 i-mol (22 A_i–A_j, 12 A_i–B_j))			
Total NOEs	548			
Hydrogen bond restraints	88			
Total restraints	636			
Restraints violations*				
NOE distances with violations >0.1 Å	6 ± 2			
NOE distances with violations >0.2 Å	1 ± 1			
NOE distances with violations >0.3 Å	0.2 ± 0.4			
AMBER94 energy, kcal·mol^{-1}	−603 ± 11			
rmsd from ideal covalent geometry				
Bonds, Å	0.0077 ± 0.0003			
Angles, °	1.834 ± 0.007			
Pairwise rmsd	A	B	A–B	(A–B)$_2$
Backbone, Å			2.61 ± 0.59[†]	2.97 ± 0.46[†]
	0.21 ± 0.01[‡]	0.30 ± 0.01[‡]	0.54 ± 0.14[‡]	0.59 ± 0.19[‡]
Heavy atoms, Å			3.59 ± 0.57[†]	3.84 ± 0.40[†]
	1.48 ± 0.32[‡]	1.83 ± 0.22[‡]	1.78 ± 0.19[‡]	1.65 ± 0.24[‡]
rmsd from average structure				
Backbone, Å	2.07 ± 0.28[†]; 0.61 ± 0.15[‡]			
Heavy atoms, Å	2.67 ± 0.23[†]; 1.35 ± 0.12[‡]			
PROCHECK NMR (G-factor and Ramachandran analysis)				
Overall G factor	−0.24[†], 0.13[‡]			
Residues in the favored region, %	85.4[†], 99.5[‡]			
Residues in the additional allowed region, %	7.4[†], 0.4[‡]			
Residues in the generously allowed region, %	0.9[†], 0.1[‡]			
Residues in the disallowed region, %	6.3[†], 0.1[‡]			

I, intra; i, inter; lr, long-range; mr, medium-range; s, sequential; mol, molecular; rmsd, rms deviation.
*No restraint violation >0.32 Å was detected.
[†]For all protein residues.
[‡]For helix residues (A/7–19, B/6–22).

BIOPHYSICS

D1 Forms a Dimer. A detailed structural study by simulated annealings including distance restraints from NOESY spectra in water clearly confirmed a conformational preference of both D1 chains for helical structures. However, qualitative analysis of large restraint violations strongly suggested the presence of a noncovalent (A–B)$_2$ homodimer, exhibiting a parallel arrangement of two A–B units, and a parallel helix orientation within each A–B molecule. Identification of symmetric parallel bundles involves the potentially dangerous assignment to interchain interactions of a subset of NOESY effects whose alternative interpretation would involve short-range intrachain interactions. In this view, an independent confirmation of D1 oligomerization status in aqueous solution was achieved by size-exclusion chromatography under the experimental conditions used for NMR analysis. At pH 5.8 and 6.8, synthetic and natural D1 eluted with an apparent molecular mass of 13 and not 5.5 kDa (Fig. 5B), as expected on the basis of the amino acid sequence, demonstrating the occurrence of D1 as a dimer.

Three-Dimensional Structure of D1. The detailed 3D structure of D1 dimer in water was obtained by assigning intra- vs. intermonomer NOEs (Table 3), with the conservative approach described in *Supporting Materials and Methods*. This procedure led to a final bundle of 24 most favorable structures (Fig. 2A), which provided quite satisfying values for an NMR structure of PROCHECK_NMR (15) G-factor values, ranging from -0.40 to -0.02, and Ramachandran plot distribution (Table 3).

An analysis of backbone atoms rms deviation, ψ, and ϕ dihedral angular order parameters (16) on the final bundle showed a very tight convergence of helical regions for all chains and a very well defined spatial arrangement of the chains within each A–B unit and between different A–B monomers (Table 3 and Table 5, which is published as supporting information on the PNAS web site). The overall 3D structure of D1 dimer in water is largely characterized by a symmetrical full-parallel, left-handed, non-coiled-coil four-helix bundle (Fig. 2B). In fact, chains A and B exhibit a largely α-helical structure, involving residues 7 to 19 (20 in 25% of the structures) for A chains and 6 (2 in 20%, 3 in 35%, 4 in 40%, 5 in 40% of the structures) to 22 (23 in 40% of the structures) for B chains. All helix pairs show a parallel orientation, with the two A chains in direct interaction, forming the core of the bundle and exhibiting almost parallel helical axes (A$_1$–A$_2$ interhelical angle: 15° $\pm$ 4°). B chains are arranged diagonally (31° $\pm$ 4° and 44° $\pm$ 3° for intra- and intermolecular A–B angles, respectively) on each side of the A$_1$–A$_2$ bundle, forming interactions with both A chains, and showing an opposite tilt (B–B angle: 75° $\pm$ 6°) with respect to the vector bisecting the A$_1$–A$_2$ helical axes, the latter representing a C_2 symmetry axis for the four-helix bundle.

Analysis of atomic interactions and residue surface accessibilities in D1 dimer showed no stable strong interchain polar interactions. On the contrary, D1 dimerization in water minimized exposure of hydrophobic residues and stabilized the largely α-helical structure. In fact, most of the large loss of solvent-accessible surface area upon dimerization (1,172 Å^2 per A–B unit, i.e., 26% of the A–B surface) derived from either interaction among hydrophobic residues or immobilization and interaction of A chain N-terminal regions with surrounding chains. Thus, formation of a hydrophobic core involving the most bulky residues of both A and B chains (Fig. 2C) appeared to be the main driving force for both relative arrangement of A to B chains and overall dimer assembly. In particular, leucines inside the core tended to cluster, whereas aromatic residues formed a stair-like arrangement, running almost perpendicular to the A$_1$–A$_2$ average helical axis (Fig. 2D). The uniform distribution of basic residues on the overall dimer surface, minimizing electrostatic repulsion among positively charged side chains, could act as a further driving force for dimerization.

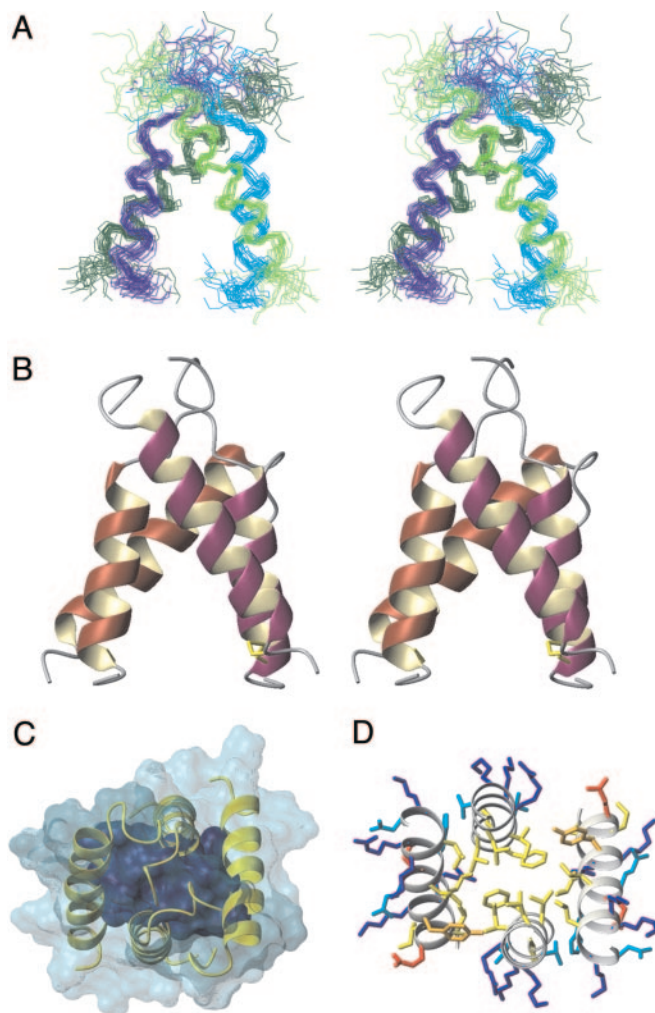The stable and well folded D1 dimeric structure observed in

Fig. 2. Dimeric structure of D1 in aqueous solution. (*A*) Backbone trace stereoplot of the final structure bundle of D1 dimer in solution. Chains A$_1$, B$_1$, A$_2$, and B$_2$ are colored in blue, dark green, cyan, and medium green, respectively. A best-fit superposition of backbone atoms of residues 7–19 for A chains and 6–22 for B chains is shown. (*B*) Ribbon stereoplot of a representative structure of the D1 dimer. A$_1$–B$_1$ and A$_2$–B$_2$ monomers are colored in purple and brown, respectively. Yellow sticks represent side-chain bonds of disulfide-linked cysteine residues. In this view, the C_2 symmetry axis of the bundle corresponds to the horizontal axis of the figure. (*C*) Solvent-accessible surface (SAS) and hydrophobic core of D1 dimer. The overall molecular SAS is shown as a semitransparent aquamarine surface. The hydrophobic core of the dimer, represented by the SAS of the hydrophobic residues, is shown as an opaque blue surface. D1 chains are represented by yellow ribbons. (*D*) Amphipathic distribution of residues in D1 dimer. Shown is the top view of the bundle with hydrophobic, uncharged polar, basic, and acidic side chains shown as yellow (orange for Y), cyan, blue, and red sticks, respectively. Residues not in helical conformation are omitted for clarity, and the backbone of helical regions is represented by gray ribbons.

water clearly suggested that the aforesaid interactions could compensate for the energetically unfavorable dipolar interactions occurring among the four parallel helices. The self-complementary hydrophobic regions within both A–B units and (A–B)$_2$ dimer, seeming at first sight unrelated to all proposed mechanisms of antimicrobial activity, prompted us to explore potential biological implications of D1 oligomerization in water. Because D1 does not present chemical functionalities (acetylation, amidation, D-amino acids, cyclization) protecting molecules from enzymatic degradation, we evaluated the possible role of dimerization in determining an increased resistance to proteases activity (1, 17).
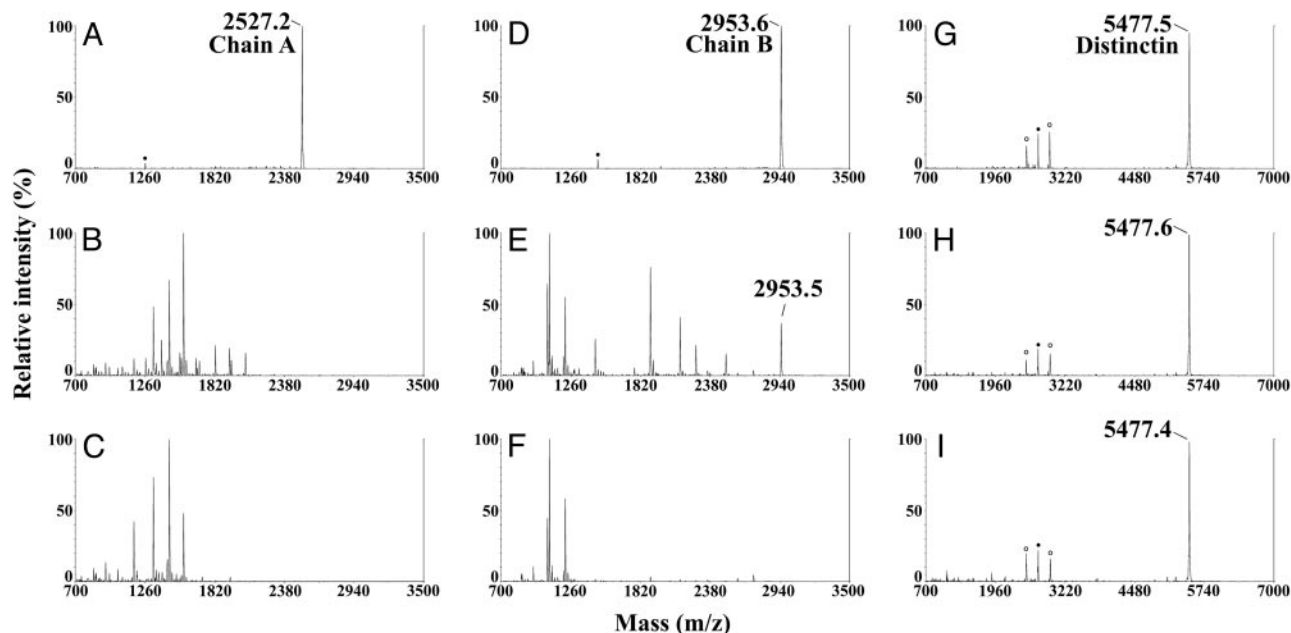
Raimondo *et al.*

Fig. 3. Comparative proteolytic degradation of D1 chain A, D1 chain B, and intact D1. Peptides (300 pmol) were incubated with 0.36 ng of trypsin in 50 mM ammonium acetate, pH 6.5, at 37°C. Aliquots (30 pmol) were withdrawn on a time-course basis and directly analyzed by MALDI-TOF MS. (*A*, *B*, and *C*) Chain A after 0, 3, and 6 h of digestion, respectively. (*D*, *E*, and *F*) Chain B after 0, 3, and 6 h of digestion, respectively. (*G*, *H*, and *I*) D1 after 0, 3, and 6 h of digestion, respectively. Filled and empty circles indicate doubly charged ions and molecular ions resulting from MALDI in-source reduction of D1, respectively. Absence of reduced peptides in D1-containing samples was verified by electrospray MS analysis.

Resistance to Protease Degradation. *In vitro* proteolysis experiments have been widely used to study of bioactive peptide inactivation by proteases and probe structured regions in polypeptides (17, 18). Then, comparative experiments on melittin, magainin II, and D1 chain A, chain B, and intact heterodimer were performed by digesting isolated peptides with equal amounts of different proteases. Aliquots were withdrawn on a time-course basis and directly analyzed by MALDI-TOF MS. A different susceptibility to degradation of intact D1 with respect to the isolated chains was evident, as clearly shown by trypsin-catalyzed hydrolysis (Fig. 3). A complete digestion of melittin and magainin II was observed under the same experimental conditions (not shown). These experiments demonstrated that, although presenting basic amino acids exposed on molecular surface (Fig. 2*D*), the four-helix bundle of D1 dimer is rigid enough to prevent extensive degradation. More evident results were obtained with chymotrypsin and subtilisin (not shown), whose activity was directed toward amino acids mainly present inside the nonpolar core of the dimer (Fig. 2 *C* and *D*).

Discussion

Antimicrobial peptides have been classified into four major groups according to their sequence and 3D structure: (*i*) linear peptides not having cysteines, (*ii*) linear peptides with a high percentage of certain residues such as Pro, Arg, or Trp, (*iii*) linear peptides presenting a cyclic moiety formed by a disulfide bond at the C terminus, and (*iv*) peptides with two or more disulfides that constrain antiparallel chains in a rigid network (1, 2). The first three classes include molecules that are unstructured in water, or generically aggregated under drastic concentration/ionic strength conditions, but present an α-helical conformation when interacting with hydrophobic media (1, 2). The fourth group includes examples presenting mainly or only β-sheet structure in aqueous solution (19, 20). In this article, we report the 3D structure of D1, a peptide that here we propose as a prototype of a previously unrecognized class of antimicrobial derivatives. In fact, NMR spectroscopy and previously unrecognized restrained molecular dynamics in aqueous

solution demonstrated that D1 presents a well defined and unique symmetrical, full-parallel, left-handed, four-helix bundle structure, formed by the noncovalent oligomerization of two 47-aa monomers, each consisting of two helices connected by the disulfide C^{19A}–C^{23B} (Fig. 2). Antimicrobial peptides with a similar fold have not been described previously, to our knowledge. In fact, hCAP-18/LL-37 and melittin, the only other peptides known to aggregate in solid or solution state, were either not structurally characterized (21) or presented a completely different fold, with a fully antiparallel bundle formed by bent helices, and pairs of almost parallel helices crossing at ≈120° (22). Moreover, a structural comparison of D1 with known structures in the Dali structural database (23), integrated by an extensive visual inspection of the Structural Classification of Proteins (SCOP) (24) and hierarchical CATH (25) fold databases, did not reveal any other protein or protein domain simultaneously exhibiting the left-handed twist, full-parallel, non-coiled-coil topology observed for D1, but only some of these structural elements. The peculiar features of D1 dimer derive from the presence/position of disulfide bridges and distribution of hydrophobic residues along the two chains. Accordingly, D1 dimer can be considered as a representative example of a novel protein fold.

Structural representations reported in Fig. 2 illustrate how the amphipathic character of each helical chain contributes to stabilize the dimeric structure of D1 in water. This figure also shows the intrinsic amphipathic potential of chain A and B that can be elicited after membrane interaction. The possibility that chains A and B should maintain a helical conformation after membrane interaction was strongly suggested by CD spectroscopy analysis, demonstrating an increase in helical content on passing from an aqueous to a hydrophobic/membrane-mimetic environment (Fig. 4 and data not shown) (7). Accordingly, D1 appears to have all of the structural features to insert and form pores in membranes by autoassociation of different molecules. D1 capability to generate pore-forming aggregates was investigated by using artificial planar lipid bilayers. The I–V curves showed unambiguously that D1 is able to permeabilize planar

lipid bilayers (Fig. 1*B*), thus explaining its strong bactericidal activity (Table 1). This behavior was confirmed by single-channel experiments because D1 induced well defined current fluctuations at different voltages (Fig. 1*C*). These experiments seem to indicate that insertion of peptide aggregates would be voltage dependent and, as soon as the peptides are embedded in the membrane, the mechanism of ion channel formation would become voltage independent. Several mechanisms have been described in the literature to explain membrane permeation by linear α-helical peptides (5), namely barrel-stave (26), toroidal pore (27), and carpet–like (28). D1 concentrations necessary for macroscopic and single-channel measurements were very low (<10 nM) and would not be compatible with the latter one. Moreover, the charge effect introduced by phosphatidylserine in a lipid bilayer did not play any role, contrarily to what was observed for cationic peptides acting according to the carpet-like mechanism (29). Finally, the observed reproducible multistate behavior at different voltages and increments between each level of conductance, which increased according to a geometric progression, are the most convincing points suggesting a barrel-stave mechanism (Table 2) (30). However, additional experiments will be necessary to definitively clarify the mechanism of membrane permeabilization by D1.

Nevertheless, the positively charged surface and extensive hydrophobic core of D1 dimer structure in water (Fig. 2) are not compatible with all the above-mentioned models, in which the molecules are commonly stabilized by interactions between the hydrophobic face of monomers and the hydrophobic moiety of lipids, with the channel formed by hydrophilic sectors of peptides. In fact, D1 structure in water seems simply designed to interact efficiently with the negatively charged head-groups of phospholipids, favoring peptide adsorption on lipid bilayer surface. On the contrary, membrane permeabilization by D1 would require (in addition to eventual changes in aggregation stoichiometry) a subsequent molecular rearrangement, most likely through a simple rotation around an axis parallel to the D1 dimer C_2 axis, consequent reversal of hydrophobic vs. hydrophilic regions exposure, and finally interaction of peptide hydrophobic portions with aliphatic moieties of membranes. The energetic cost of this conformational change, probably correlated to the high voltages observed to embed peptide in phospholipids and generate ion channels, is substantially reduced by the full-parallel helical arrangement of D1 dimer, which implies disruption of unfavorable electrostatic interactions among parallel helical dipoles. Although D1 structure in water indicates that the helical portion of chain B is long enough to span a membrane and form the bundle, additional NMR studies in membrane-mimetic media will be necessary to structurally elucidate the conducting aggregates, determining the exact role of chain A in bilayer permeabilization.

The most direct and innovative implication for the understanding of antimicrobial peptide structure–function relationships is the potential role of the fold and aggregation observed for D1 in water on molecular transport and stability properties. In fact, when a simple D1 A–B monomer is considered, it exhibits a relatively high content of hydrophobic residues, with a potential amphipathic distribution. All these features frequently give rise to unfolding, precipitation, or aggregation in water. This disorder should greatly favor peptide degradation (17), as demonstrated by proteolysis experiments (Fig. 3). All together, these phenomena could affect adversely the activity *in vivo* of D1 as an antimicrobial agent. Many antibiotic peptides are made resistant to degradation by posttranslational modifications (1–4). The peculiar fold and dimerization pattern of D1 suggest a different stabilization and solubilization mechanism, based on a transport form of the peptide that is considerably more compact and resistant than any possible structure of simple monomers, with a well-secluded hydrophobic core and a rather uniform surface distribution of basic residues. All these features reduce problems such as extensive aggregation, random adhesion to hydrophobic surfaces, or enzymatic degradation.

The growing problem of microbial resistance to conventional antibiotics and the need for new compounds with antibiotic properties have stimulated interest in the development of novel antimicrobial peptides. In this scenario, D1 appears to be an interesting prototype for the design and development of novel dimeric antimicrobial agents. Recently, different groups reported that disulfide-dimerized analogues of linear α-helical peptides present an enhanced binding to membranes, low concentration dependence for membrane permeabilization, and larger pore-formation capability than monomers (31, 32). It has also been demonstrated that magainin II dimerizes upon binding to phospholipid bilayers (33). Moreover, other nonhelical peptides having a dimeric structure to increase diversity have been recently isolated in murine small intestine tissues (10). All these studies strongly suggest that dimerization might be a powerful modification to strengthen the activity of monomeric species as well as increase the repertoire of action (34). In this article, we propose an additional role of covalent heterodimerization and/or noncovalent oligomerization in peptide antimicrobial activity: resistance against degradation by bacterial proteases. Further studies are needed to determine the 3D structure of D1 in a membrane-like environment, in an attempt to advance our knowledge of structure–activity relationships and design new derivatives with enhanced antimicrobial properties.

1. Zasloff, M. (2002) *Nature* **415,** 389–395.
2. Hancock, R. E. & Lehrer, R. (1998) *Trends Biotechnol.* **16,** 82–88.
3. Boman, H. G. (2003) *J. Intern. Med.* **254,** 197–215.
4. Barra, D. & Simmaco, M. (1995) *Trends Biotechnol.* **13,** 205–209.
5. Oren, Z. & Shai, Y. (1999) *Biopolymers* **47,** 451–463.
6. Rinaldi, A. C. (2002) *Curr. Opin. Chem. Biol.* **6,** 799–804.
7. Batista, C. V., Scaloni, A., Rigden, D. J., Silva, L. R., Rodrigues Romero, A., Dukor, R., Sebben, A., Talamo, F. & Bloch, C. (2001) *FEBS Lett.* **494,** 85–89.
8. Lee, I. H., Lee, Y. S., Kim, C. H., Kim, C. R., Hong, T., Menzel, L., Boo, L. M., Pohl, J., Sherman, M. A., Waring, A. & Lehrer, R. I. (2001) *Biochim. Biophys. Acta* **1527,** 141–148.
9. Jang, W. S., Kim, K. N., Lee, Y. S., Nam, M. H. & Lee, I. H. (2002) *FEBS Lett.* **521,** 81–86.
10. Hornef, M., Putsep, K., Karlsson, J., Refai, E. & Andersson, M. (2004) *Nat. Immunol.* **5,** 836–843.
11. D'Ambrosio, C., Talamo, F., Vitale, R. M., Amodeo, P., Tell, G., Ferrara, L. & Scaloni, A. (2003) *Biochemistry* **42,** 4430–4443.
12. Hall, J. E., Vodyanoy, I., Balasubramanian, T. M. & Marshall, G. R. (1984) *Biophys. J.* **45,** 233–247.
13. Montal, M. & Mueller, P. (1972) *Proc. Natl. Acad. Sci. USA* **69,** 3561–3566.
14. Hanke, W. & Kaupp, U. B. (1984) *Biophys. J.* **46,** 587–595.
15. Hwang, T. L. & Shaka, A. J. (1995) *J. Magn. Reson.* **112,** 275–279.
16. Hyberts, S. G., Goldberg, M. S., Havel, T. F. & Wagner, G. (1992) *Protein Sci.* **1,** 736–751.
17. Yeaman, M. R. & Yount, N. Y. (2003) *Pharmacol. Rev.* **55,** 27–55.
18. Fontana, A., Polverino de Laureto, P., De Filippis, V., Scaramella, E. & Zambonin, M. (1997) *Folding Des.* **2,** R17–R26.
19. Schibli, D. J., Hunter, H. N., Aseyev, V., Starner, T. D., Wiencek, J. M., McCray, P. B., Tack, B. F. & Vogel, H. J. (2002) *J. Biol. Chem.* **277,** 8279–8289.
20. Yang, Y., Poncet, J., Garnier, J., Zatylny, C., Bachere, E. & Aumelas, A. (2003) *J. Biol. Chem.* **278,** 36859–36867.
21. Oren, Z., Lerman, J., Gudmundsson, G. H., Agerberth, B. & Shai, Y. (1999) *Biochem. J.* **341,** 501–513.
22. Terwilliger, T. C. & Eisenberg, D. (1982) *J. Biol. Chem.* **257,** 6010–6015.
23. Holm, L. & Sander, C. (2003) *J. Mol. Biol.* **233,** 123–138.
24. Murzin A. G., Brenner S. E., Hubbard T. & Chothia, C. (1995) *J. Mol. Biol.* **247,** 536–540.
25. Orengo, C. A., Michie, A. D., Jones, S., Jones, D. T., Swindells, M. B. & Thornton, J. M. (1997) *Structure* **5,** 1093–1108.
26. Baumann, G. & Mueller, P. (1974) *J. Supramol. Struct.* **2,** 538–557.
27. Huang, H. W. (2000) *Biochemistry* **39,** 8347–8352.
28. Shai, Y. (1999) *Biochim. Biophys. Acta* **1462,** 55–70.
29. Powers, J. S. & Hancock, R. E. W. (2003) *Peptides* **24,** 1681–1691.
30. Saint, N., Marri, L., Marchini, D. & Molle, G. (2003) *Peptides* **24,** 1779–1784.
31. Dempsey, C. E., Ueno, S. & Avison, M. B. (2003) *Biochemistry* **42,** 402–409.
32. Wakamatsu, K., Takeda, A., Tachi, T. & Matsuzaki, K. (2002) *Biopolymers* **64,** 314–327.
33. Hara, T., Kodama, H., Kondo, M., Wakamatsu, K., Takeda, A., Tachi, T. & Matsuzaki, K. (2001) *Biopolymers* **58,** 437–446.
34. Lehrer, R. I. (2004) *Nat. Immunol.* **5,** 775–776.

Raimondo *et al.*